Dr. Arnaud Mignan
Institute of Geophysics,
Swiss Federal Institute of Technology, Zürich
NO H66, Sonneggstrasse 5
CH-8092 Zürich
arnaud.mignan@sed.ethz.ch

5 December 2017

Dear Editor and Reviewers,

Please find below my answers to your comments, as given in the discussion section of NPG. I now additionally refer to line numbers of the annotated version of the modified manuscript to describe specific changes. Those additions are highlighted in blue in the present reply. The main changes made to the article are the addition of two new subsections (2.2 and 3.2 on the aftershock spatial distribution) and of two new figures (Figs. 4-5).

Sincerely,

Arnaud Mignan

Anonymous Referee #1

The MS presented by Dr. Mignan intends to provide the background of the aftershock productivity law where the number of aftershock is proportional to the exponential of the magnitude (M) of a mainshock. On the basis of "Solid Seismicity Postulate"(SSP), the author derives the formula of the expected number of aftershocks as a function of M which agrees with the productivity law originally suggested by Utsu [1970]. The derived formula has a break in the log-linear relationship between the aftershock productivity and M whereas the break is not found through the analysis of real aftershock data. The author suggests that this inconsistency is caused by an aftershock selection bias with a numerical simulation.

I have two major concerns on this MS as shown below. a) I do not understand well what new significant results are in this MS. In Hainzl et al [2010, JGR], the aftershock productivity law has already been reproduced with a numerical simulation. The simulation is based on the "clock-advanced" model, which is a simple but realistic physical assumption. By contrast, SSP is too simple, and because of this simplification its physical background seems obscure and unrealistic. Furthermore, the postulate has not been supported by real data (In some of the author's previous papers, seismicity model derived from SSP has been applied to real seismicity data.

Note that, however, only temporal patterns of seismic activity are analyzed. To validate SSP where we have only three seismicity levels in space, it is indispensable to reproduce spatial patterns of real earthquakes.). This MS does not show any convincing motivation to explain the productivity law with such an unsupported postulate. I understand that sometimes it is important to introduce a (too) simple model/assumption for explaining an empirical law. However, it is also important to provide some new and meaningful perspective as a result of the introduction. The results shown in this MS do not go beyond the results of Hainzl et al. [2010], and therefore the introduction of SSP is unproductive.

b) In the end of Section 3, the author suggests the break in scaling in the after- shock productivity data (Eq.(16)). However, as a result of the analysis of the real aftershock data, no break is found (L.182-183). To explain the result of "no break", in Section 4 the numerical simulation with the ETAS model was conducted. Then, the author ascribes this result to the "aftershock selection bias" (L.206-207) in the numerical simulation. The author's conclusion is one possibility, but it is also possible that Eq.(16) is incorrect; the numerical simulation shown in Section 4 is inconclusive, and I do not understand what is the meaning of showing such a vague consequence. The application of an aftershock selection approach having a serious problem (the bias in this case) itself is inappropriate. Why does the author use any other approach which does not contain such a problem? In other words, only a negative possibility for the postulate is shown and no positive support is not given in the present form of this MS. To my opinion, this is another major drawback of this MS.

Some further comments:

1) Introduction of the Zero-Inflated Poisson (ZIP) distribution The reason of the introduction of the ZIP distribution is described in L.165-166 ("this approach ... zero aftershock"), but this explanation seems insufficient. Behind the ZIP distribution, we have the following assumption. We have two possibilities: the first is that the number of events follows a Poisson distribution, and the second is that it is deterministically equal to zero. One of these two possibilities is chosen through the Bernoulli distribution. As far as I know, a physical (seismological) process corresponding to the Bernoulli distribution is unclear in generating earthquakes. If the author persists in introducing the ZIP distribution, explain what is the physical process.

2) The simulation shown in Section 4 This simulation is based on the ETAS model, and this violates the self-consistency of this MS. As seen in $g(x,y|M)$ of Eq.(17), the spatial density of aftershocks gradually decays with the distance from a parent event. This property completely disagree with SSP (see Eq.(5)). For the self-consistency, the simulated spatial (and temporal) pattern of earthquakes should be generated on the basis of SSP.

3) α = 2.04 (L.197) I do not understand how the author incorporated this information (value) into Eq.(16).

Reply to Anonymous Referee #1

Dear reviewer,

Thank you for your comments on the discussion paper by Mignan (2017). Below is my two-part answer to (1) show that the Solid Seismicity Postulate is supported by seismicity data and (2) discuss in more detail the mismatch between theoretical scaling break and lack of break in real data. A third section answers to your other comments.

1 Support of the Solid Seismicity Postulate (SSP) by aftershock data

The SSP should indeed be verified to be consistent with the spatial distribution of seismicity data (see new results in abstract lines 16-20). I first clarify that the step-like function of event density in space is only expected for the case of an idealised smooth static stress field (lines 163-165). I now compare this case (new Fig. 4a-b) with the case of a stress field with uniform noise (Fig. 4c-d). While the ideal case is used to develop analytical solutions, a heterogeneous stress field described by additive uniform noise was already used in past studies to simulate non-stationary background events (King and Bowman, 2003; Mignan et al., 2007; Mignan, 2011). Addition of such noise blurs the "aftershock solid", which reflects in the aftershock spatial density distribution, switching from a step function to a power-law of the form $\rho(r) \propto r^{-q}$, with ρ the linear spatial density and exponent $q = 1.96$ (the 1.7 value given in the discussion post was erroneous, as I had used the wrong MLE formulation – both values remain within the q-range given in the literature. q = 1.96 better fits the tail of the power-law as shown in Fig. 4d). Figure 4 was inserted in the revised manuscript and a new subsection added, titled "2.2. Validation of the Solid Seismicity Postulate" (lines 162-189).

As shown in Figure 5 in the revised manuscript, the power law exponent obtained from the SSP with noisy static stress field matches the power law exponent found in Southern California. In the literature, $1.3 < q < 2.5$ was found for California (Felzer and Brodsky, 2006; Lipiello et al., 2009; Marsan and Lengliné, 2010; Richards-Dinger et al., 2010; Shearer, 2012; Gu et al., 2013; Moradpour et al., 2014; van der Elst and Shaw, 2015). This demonstrates that the SSP is not "*too simple*" or "*unrealistic*". Comparison of Figure 4d with Figure 5a shows that "*the spatial patterns of real earthquakes are reproduced*" by the SSP (i.e., the power-law behaviour) with a realistic q-value (without any tuning required). A short review of past studies on the spatial distribution of aftershocks is now given lines 168-174 and a discussion of Figure 5 added in the new section 3.2 "Aftershock spatial density distribution" (lines 202-236) of the revised manuscript (section 3 "Observations & Model Fitting" being now separated in 3 subsections).

This work goes beyond the results of Hainzl et al. (2010) since an analytical formulation is explicit while the physical driver of a simulation output is implicit and potentially ambiguous (see new results in abstract lines 26-28). In the King and Bowman (2003) study for example, a power-law behaviour of precursory seismicity emerged from their static stress simulations. However the result was ambiguous. It was not clear if the behaviour emerged from the stress field geometry, implemented Gutenberg-Richter power-law, or else. It led to the first study on Solid Seismicity, which demonstrated that the power-law time-to-failure equation derived from the geometry of the stress field (Mignan et al., 2007). While such ambiguity may not be present in the simulations of Hainzl et al. (2010), we are still left wondering which parameters are critical to the emergence of the Utsu productivity law, i.e., "*it remains unclear how K_0 and α relate to the underlying physical parameters*" (line 50).

Here are two "*new and meaningful perspectives as a result of the introduction*" of the SSP (new section 3.2 and extended section 3.3, new figure 5):

(*i*) It is first of importance to demonstrate that the Solid Seismicity theory can explain the aftershock productivity law, since it already explains both tectonic foreshocks (Mignan, 2012) and induced seismicity (Mignan, 2016). If such physical framework can explain the main seismicity patterns observed in Nature, it becomes a potential candidate for a unified theory of seismicity.

(*ii*) Figure 5 (and the new section 3.2 and extended section 3.3) goes farer into the Solid Seismicity analysis, showing how to estimate its main parameters (intermediary parameter r_*, main parameters δ_+ and $\Delta\sigma_*$). We first note that the q = 1.96 theoretical estimate (SSP + uniform noise) is compatible with observations (Fig. 5a). I here focus on the largest mainshocks to avoid the scattering and scaling break issues at small M. On the same plot, we can roughly estimate r_* = 1 km (maximum r at which the ρ plateau breaks – in analogy with Fig. 4d). It is constant for any large M (> M_{break}) since the stress drop is a constant, $c = w_0$ is a constant, and $\Delta\sigma_*$ is also *a priori* a constant (one of the 2 main parameters of the Solid Seismicity approach; Eq. 7). See lines 215-218 (section 3.2). Now let us calculate δ_+ from the commonly used parameter K_0 (section 3.3 lines 238-301). We first note from Eq. (11) that the second term is negligible for large M, yielding

$$K(M > M_{break}) \approx 2\delta_+(m_0) r_* \exp[ln(10)(M-4)] \qquad \text{(X1 – new 18)}$$

Rearranging m_0 and M-4 and comparing to the original Utsu Eq. (1), we get

$$\delta_+(m_0) = \frac{K_0 \exp[\ln(10)(4-m_0)]}{2r_*} \qquad \text{(X2 – new 19)}$$

With $\alpha = \ln(10)$ fixed and K_0 estimated from the MLE for $M > 6$, we get $K_0 = 0.025$ and thus $\delta_+(m_0 = 2) = 1.23$ events/km^3 (fit represented in Fig. 5b). If correct, the linear density below r_* (plateau) for any given large M should be

$$\rho(r < r_*, M) = \delta_+ \exp[\ln(10)(M - 4)] \quad \text{(X3 – new 14)}$$

which is represented on Fig. 5a and matches the data (Eq. (14) simply calculates the linear density of events ρ from the volumetric density of events δ_+) (lines 222-228). This suggests that δ_+ is also constant, at least for the four largest strike-slip mainshocks in Southern California (line 297). One could have also estimated δ_+ directly from $\rho(r)$ (as done for r_*) to directly derive the aftershock productivity law of Southern California with Eq. (18). This shows the direct link between aftershock productivity and aftershock spatial distribution (or geometry). As for the parameter $\Delta\sigma_*$, its estimation remains ambiguous as it depends on the seismogenic width w_0. We get the ratio $\Delta\sigma_*/\Delta\sigma_0 = \{-0.5, -1.0, -1.4\}$ for $w_0 = \{5, 10, 15\}$ km, respectively (Eq. 7) (lines 218-221).

This of course remains a preliminary analysis. However I hope that additional analyses of aftershocks, foreshocks as well as induced seismicity in different regions will provide useful information as to the distribution of the $\Delta\sigma_*$ and δ_+ parameters. Are they universal? Is a same regional value applicable to all types of seismicity? Are there any correlations? Those are important questions I wish to answer in the near future. To do so, the theoretical framework must first be conveyed for each class of seismicity pattern. See lines 363-368 in the conclusion.

2 Theoretical scaling break & mismatch with seismicity data

The discussion paper already indicates that: "*Possible biases of aftershock selection may explain the lack of break*" (lines 18-20, abstract) and "*while such a bias is possible, it yet does not prove that the break in scaling exists*" (line 208) – This clearly suggests that it is only one possible option. It is indeed a weak argument (since based on a negative result) but it is so far the best one available (all existing declustering techniques assuming no break in magnitude). "*It is also possible that Eq. (16) is incorrect*", true, but so would the clock-advance model in such premise, which the reviewer describes as "*a simple but realistic physical assumption*". No explanation for the lack of break in real data was given in Hainzl et al. (2010). The present paper provides one possible explanation. Any criticism on the scaling break mismatch shall apply the same way to the present study and the published one of Hainzl et al. (2010). An alternative view is that both studies found the same scaling break, hence supporting this result as characteristic of the static stress process.

Following on the new results presented in Figure 4d, the explanation of lack of break due to aftershock selection bias becomes a more realistic one. It is NOT "*a vague consequence*" since any study of the aftershock productivity law is based on the use of such a declustering method. The ETAS simulation does NOT "*violate the self-consistency of this MS*" since the power-law spatial distribution is now shown to be verified by the SSP (line 321). The theoretical value q = 1.96 is close to the value I already used in the ETAS simulations (q = 1.47) and observed here for the largest strike-slip mainshocks (Fig. 5a). Since the aftershock selection bias is only one option, another alternative is now discussed: The proposed productivity equation assumes moment magnitude while the earthquake catalogue is in local magnitude. Deichmann (2017) recently demonstrated that while $M_L \propto M_w$ at large M, $M_L \propto 1.5M_w$ at small M. This would cancel the kink observed in the real data. However the scaling break predicted by Deichmann (2017) occurs at several magnitude units below the geometric one expected by static stress (new lines 348-354).

3 Other aspects

On the introduction of the Zero-Inflated Poisson (ZIP) distribution: Explaining the distribution of earthquakes, from the static stress process to their occurrence on a fractal network of faults remains out of the scope of the present study. Since the ZIP does not lead to significant changes in the α-value and since section 3 is now completed with an analysis of the spatial distribution of aftershocks, the ZIP part has been deleted from the revised manuscript.

On α = 2.04 (line 197): This is the maximum likelihood estimate of α obtained for Southern California in the present study (see line 164). α is thus constrained from large magnitude data (Fig. 4a) and the simulated break at lower magnitudes is estimated from the theoretical value 3/2 α. Values of α are now given for different magnitude M ranges and explained (lines 248-250, 309-313, 334).

Anonymous Referee #2

This is an interesting paper which correlates the Utsu aftershock productivity with the geometric operations on the permanent static stress field. The paper is well written and I have very minor comments on the manuscript as indicated below.

1. For Figure 2, several hours after the 1992 Landers earthquake, the largest aftershock (or triggered earthquake), Big Bear earthquake, occurred southwest of the mainshock source region. I think it's better to mention in the text (around Lines 90) that these off-fault triggered seismicity also happened due to static stress changes imparted by the mainshock, while these triggered seismicity are out of topic in this paper. (If my understanding is correct, please neglect if I'm wrong) 2. In Figure 2a, the author assumed the regional stress of 10 bar. But, I think that this assumed

regional stress is too small to cause earthquakes, because a stress drop basically ranges 10-100 bars (Kanamori and Anderson). Furthermore, I think that it is not so obvious whether on- fault aftershocks are due to static stress changes imparted by the mainshock or not. It's better to mention this point more carefully by referring several previous studies.

Reply to Anonymous Referee #2

Dear reviewer,

Thank you for your comments on the discussion paper by Mignan (2017).

As per your suggestion, I now mention the case of triggered off-fault seismicity, as exemplified by the Big Bear earthquake, which is indeed "also due to static stress changes imparted by the mainshock". The anisotropic effects observed on nearby faults can be explained by the Solid Seismicity Postulate, as shown already in Figure 5 of Mignan (2016). This is now explained in the text. Since such heterogeneities in space are not systematic, they are indeed "out of topic in this paper", which is concerned with the general productivity law that applies to all mainshocks on average. See new lines 229-236 and new curve in Figure 5a.

Regarding Figure 2a, 10-bars seems like a reasonable value for a stress drop. Looking at Figure 5 of Abercrombie and Leary (1993), observations are centred on 1-100 bar in log10 scale. Then Figure 2a represents the case where the stress drop counterbalances the regional deviatoric stress, so whatever value is used, the final outcome would be the same (Figures 2a and 2d being similar to Figure 3 of King et al., 1994). Finally, a reference to Miller et al. (2004) has been added to indicate that additional physical processes (such as trapped high pressure gas) may also explain part of the on-fault aftershock activity (line 384).

Referee N. Wetzler

The manuscript examines the empirical relationship of the power law aftershock productivity law. The author introduces (not only in this study) the Solid Seismicity Postulate (SSP) to predict the first order mainshock's geometrical static stress perturbation on the crustal ambient stress. The model defines two basic ruptures with respect to the free surface predicting a magnitude dependent deficiency when the rupture hits the surface. Using this physical model he explains the empirical observation. The manuscript is written well and figures are useful. I have two general comments: 1) The role of dynamic triggering. In general aftershock productivity is a product of the static and dynamic perturbation superimposed on the regional seismic susceptibility, or faults state [Dieterich, 1994]. Many examples for both dynamic triggering and Coulomb stress explain aftershocks occurrence. Due to the rapid decay of the static stress field, cases of "pure" dynamic triggering are common beyond several fault dimensions rom the mainshock [e.g. Fan and Shearer, 2016]. In the periphery of the fault, the Coulomb stress field and dynamic stress field overlap with a similar fashion, and it is unclear how they interact. My main concern is that the author does not discuss the contribution of dynamic triggering to the aftershock productivity. Does the fact that the predicted "kink" in the aftershock productivity from the geometrical interaction with the surface is due to enhancement of the dynamic triggering? 2) The geometry of the SSP. The first order shape of the SSP is not obvious to me. The geometry of the induced area is predicting a volumetric increase in static stress changes along the rupture area (red in Figure. 3). The rupture of faulted area is the expression of the coseismic slip responding to the elastic rebound. This predicts different degrees of relaxation with respect to the main- shock magnitude and the occurrence of the event in the seismic cycle. In the case of "complete" stress drop the rupture area is predicted to present spatial deficiency in productivity and some variations in the field with respect to the fault complexity. Several papers demonstrate the deficiency in aftershocks at the asperity with the majority of the seismicity focused on the periphery of the fault [Hasegawa et al., 2012; van der Elst and Shaw, 2015; Ross et al., 2017] represented by the orange volume in Figure. 3. My concern is that this model (SSP) is too simplified and does not incorporate basic modern observations.

3) Further clarification regarding the time and spatial windows used for aftershock counting for the case of Southern California is needed

Dieterich, J. H. (1994), A constitutive law for rate of earthquake production and its application to earthquake clustering, J. Geophys. Res., 99(B2), 2601–2618, doi:10.1029/93JB02581. van der Elst, N. J., and B. E. Shaw (2015), Larger aftershocks happen farther away: Nonseparability of magnitude and spatial distributions of aftershocks, Geophys. Res. Lett., 42(14), 5771–5778, doi:10.1002/2015GL064734. Fan, W., and P. M. Shearer (2016), Local near instantaneously dynamically triggered aftershocks of large earthquakes, Science (80-.)., 353(6304), 1133–1136, doi:10.1126/science.aag0013. Hasegawa, A., K. Yoshida, Y. Asano, T. Okada, T. Iinuma, and Y. Ito (2012), Change in stress field after the 2011 great Tohoku-Oki earth- quake, Earth Planet. Sci. Lett., 355–356, 231–243, doi:10.1016/j.epsl.2012.08.042. Ross, Z. E., H. Kanamori, and E. Hauksson (2017), Anomalously large complete stress drop during the 2016 M w 5.2 Borrego Springs earthquake inferred by wave- form modeling and near-source aftershock deficit, Geophys. Res. Lett., 1–8, doi:10.1002/2017GL073338.

Reply to Referee N. Wetzler

Dear reviewer,

Thank you for your comments on the discussion paper by Mignan (2017). Below is my two-part answer:

1 Regarding the potential role of dynamic stress triggering

The possible contribution of dynamic triggering to aftershock productivity is now discussed in the revised manuscript (lines 171-177):

It must first be indicated that the debate around the static or dynamic origin of aftershocks has been based on the analysis of the power-law exponent of the spatial density of aftershocks (Felzer and Brodsky, 2006; Lipiello et al., 2009; Marsan and Lengliné, 2010; Richards-Dinger et al., 2010; Shearer, 2012; Gu et al., 2013; Moradpour et al., 2014; van der Elst and Shaw, 2015). However the original claim of a dynamic origin (Felzer and Brodsky, 2006) was later on discredited (Richards-Dinger et al., 2010) and static stress is at present the favoured theory to explain aftershock distribution in space (e.g., Moradpour et al., 2014; van der Elst and Shaw, 2015) (lines 171-177 of the new section 2.2).

I now also show the observed aftershock spatial distribution to support Solid Seismicity. From the SSP, and adding a uniform noise to the regional static stress field, I find a power law exponent q = 1.96, in agreement with the Southern California aftershock data and the literature on static stress (see my reply to reviewer #1 where I show the spatial distribution of aftershocks expected by the SSP and observed; Figs. 4d; 5a). This result is now be emphasized in both abstract (lines 16-20) and main text (new sections 2.2 and 3.2, lines 321, 371-373).

Regarding the triggering of large remote events by dynamic stress (e.g., Fan and Shearer, 2016), those events have never been counted in the productivity law, declustering techniques being based on strong time-space-magnitude correlations. Even if the events shown to be triggered by dynamic stress were considered in the productivity curve, the total number of aftershocks would overshadow their role in the productivity law characteristics. Indeed, Fan and Shearer (2016) suggested the triggering of one or two M7+ aftershocks by dynamic stress per M7+ mainshock. This low number is dwarfed by the 1,000s of aftershocks produced by such mainshocks (lines 174-177).

What I infer is that static stress is sufficient to explain most of the aftershock observations over a large magnitude range, such as the aftershock spatial distribution and the aftershock productivity.

2 Regarding the geometry of the aftershock solids

The SSP expects the majority of aftershocks to occur in a volume centred on the mainshock rupture, which is clearly the case for the largest mainshocks in Southern California (Fig. 2c). This is also evident when looking at the density of aftershocks as a function of distance from rupture (new Fig. 5a – see reply to review #1). Those are "*basic modern observations*" that cannot be easily rejected.

The result of Ross et al. (2017) was already mentioned in the text and explained as a case in which the stress would only be partially relieved by the mainshock (line 97). Although other studies have found a deficiency of aftershocks on the main asperity, those works remain anecdotal and so cannot be considered "basic" (one M5.2 event in Ross et al.; Great 2011 Tohoku earthquake in Hasegawa et al., a giant earthquake that might show an anomalous behaviour). Figure 2c and 5a prove that it is not the case for the four major mainshocks in Southern California. Looking at smaller aftershock clusters also show no quiescence at the location of the mainshock. The red area shown in Figure 3 is also in agreement with the theory of static stress transfer (Fig. 2a-d), as described by the seminal paper of King et al. (1994). Finally, Solid Seismicity can still explain those anomalous behaviours. The aftershock deficiency case would mean that the term representative of the red volume is null, hence changing the shape of the productivity law (so the SSP is NOT "*too simplified*"). Unfortunately, two cases (Ross et al., 2017; Hasegawa et al., 2012) are not enough to populate such altered aftershock productivity dataset and test what modified productivity law would emerge (at least hundreds of cases would be needed) (lines 174-177).

Concerning the mentioned study of van der Elst and Shaw (2015), they do not infer a deficiency of aftershocks on the mainshock fault rupture, only a deficiency in large magnitudes. This is independent of the Solid Seismicity application shown here, where only the total aftershock count is considered. In fact, van der Elst and Shaw (2015) verified that the "*aftershock spatial decay is dominated by static stress transfer in the near field (several rupture lengths)*" and they found q = 1.77 in California in good agreement with the SSP (see reply to review #1). This goes again against the dynamic stress alternative discussed in point 1. Reference to van der Elst and Shaw (2015) has been added.

On the last point ("*further clarification regarding the time and spatial window used for aftershock counting for the case of Southern California is needed*"), it is now clarified in the revised version of the manuscript that the nearest-neighbour method is used, with only first generation aftershocks considered. This is now used systematically and figures have been updated accordingly, where needed (lines 197, 229-233, Figs. 5, 6).

Utsu aftershock productivity law explained from geometric operations on the permanent static stress field of mainshocks

Arnaud Mignan*

Institute of Geophysics, Swiss Federal Institute of Technology, Zurich

Address: ETHZ, Institute of Geophysics, NO H66, Sonneggstrasse 5, CH-8092 Zurich

Correspondence to: arnaud.mignan@sed.ethz.ch

Abstract: The aftershock productivity law is an exponential function of the form $K \propto \exp(\alpha M)$ with K the number of aftershocks, M the mainshock magnitude, and $\alpha \approx \ln(10)$ the productivity parameter. This law remains empirical in nature although it has also been retrieved in static stress simulations. Here, we explain this law based on Solid Seismicity, a geometrical theory of seismicity where seismicity patterns are described by mathematical expressions obtained from geometric operations on a permanent static stress field. We first validate the Solid Seismicity Postulate that relates seismicity density to a static stress step function. We show that it yields a power exponent q = 1.96±0.01 for the power-law spatial linear density distribution of aftershocks, once uniform noise is added to the static stress field, in agreement with observations. We then recover the exponential function of the productivity law with a break in scaling obtained between small and large M, with $\alpha = 1.5\ln(10)$ and $\ln(10)$, respectively, in agreement with results from previous static stress simulations. Possible biases of aftershock selection, verified to exist in Epidemic-Type Aftershock Sequence (ETAS) simulations, may explain the lack of break in scaling observed in seismicity catalogues. The existence of the theoretical kink remaining to be proven, we describe how to estimate the Solid Seismicity parameters (activation density δ_+, aftershock solid envelope r_* and background stress amplitude range Δo_*) for large M values only.

Arnaud Mignan 28.11.2017 10:15
Deleted: therefore

Arnaud Mignan 28.11.2017 10:15
Deleted: s

Arnaud Mignan 28.11.2017 10:15
Deleted: .

1. Introduction

Aftershocks, the most robust patterns observed in seismicity, are characterized by three empirical laws, which are functions of time (e.g., Utsu et al., 1995; Mignan, 2015), space (e.g., Richards-Dinger et al., 2010; Moradpour et al., 2014) and mainshock magnitude (Utsu, 1970a; b; Ogata, 1988). The present study focuses on the latter relationship, i.e., the Utsu aftershock productivity law, which describes the total number of aftershocks K produced by a mainshock of magnitude M as

$$K(M) = K_0 \exp[\alpha(M - m_0)] \tag{1}$$

with m_0 the minimum magnitude cutoff (Utsu, 1970b; Ogata, 1988). This relationship was originally proposed by Utsu (1970a; b) by combining two other empirical laws, the Gutenberg-Richter relationship (Gutenberg and Richter, 1944) and Båth's law (Båth, 1964), respectively:

$$\begin{cases} N(\geq m) = A\exp[-\beta(m - m_0)] \\ \qquad N(\geq M - \Delta \mathrm{m}_B) = 1 \end{cases} \tag{2}$$

with β the magnitude size ratio (or $b = \beta/\ln(10)$ in base-10 logarithmic scale) and Δm_B the magnitude difference between the mainshock and its largest aftershock, such that

$$K(M) = N(\geq m_0 | M) = \exp(-\beta \Delta \mathrm{m}_B) \exp[\beta(M - m_0)] \tag{3}$$

with $K_0 = \exp(-\beta \Delta \mathrm{m}_B)$ and $\alpha \equiv \beta$. Eq. (3) was only implicit in Utsu (1970a) and not exploited in Utsu (1970b) where K_0 was fitted independently of the value taken by Båth's parameter Δm_B. The α-value was in turn decoupled from the β–value in later studies (e.g., Seif et al. (2017) and references therein).

Although it seems obvious that Eq. (1) can be explained geometrically if the volume of the aftershock zone is correlated to the mainshock surface area S with

$$S(M) = 10^{M-4} = \exp[\ln(10)(M - 4)] \tag{4}$$

(Kanamori and Anderson, 1975; Yamanaka and Shimazaki, 1990; Helmstetter, 2003), there is so far no analytical, physical expression of Eq. (1) available. Although Hainzl et al. (2010) retrieved the exponential behavior in numerical simulations where aftershocks were produced by the permanent static stress field of mainshocks of different magnitudes, it remains unclear how K_0 and α relate to the underlying physical parameters.

Arnaud Mignan 28.11.2017 10:17
Deleted: =

The aim of the present article is to explain the Utsu aftershock productivity equation (Eq. 1) by applying a geometrical theory of seismicity (or "Solid Seismicity"), which has already been shown to effectively explain other empirical laws of both natural and induced seismicity from simple geometric operations on a permanent static stress field (Mignan, 2012; 2016a). The theory is applied here for the first time to the case of aftershocks.

2. Physical Expression of the Aftershock Productivity Law

2.1. Demonstration by Solid Seismicity

"Solid Seismicity", a geometrical theory of seismicity, is based on the following Postulate (Mignan et al., 2007; Mignan, 2008, 2012; 2016a):

> **Solid Seismicity Postulate (SSP):** *Seismicity can be strictly categorized into three regimes of constant spatiotemporal densities – background δ_0, quiescence δ_- and activation δ_+ (with $\delta_- \ll \delta_0 \ll \delta_+$) - occurring respective to the static stress step function:*
>
> $$\delta(\sigma) = \begin{cases} \delta_- & , \sigma < -\Delta o_* \\ \delta_0 & , \sigma \leq |\pm\Delta o_*| \\ \delta_+ & , \sigma > \Delta o_* \end{cases} \quad (5)$$
>
> *with Δo_* the background stress amplitude range.*

Based on this Postulate, Mignan (2012) demonstrated the power-law behavior of precursory seismicity in agreement with the observed time-to-failure equation (Varnes, 1989), while Mignan (2016a) demonstrated both the observed parabolic spatiotemporal front and the linear relationship with injection-flow-rate of induced seismicity (Shapiro and Dinske, 2009). It remains unclear whether the SSP has a physical origin or not. If not, it would still represent a reasonable approximation of the linear relationship between event production and static stress field in a simple clock-change model (Hainzl et al., 2010) (Fig. 1a) (for the validation of the SSP from the observed spatial distribution of aftershocks, see section 2.2). The power of Eq. (5) is that it allows defining seismicity patterns in terms of "solids" described by the spatial envelope $r_* = r(\sigma = \pm\Delta o_*)$. The spatiotemporal rate of seismicity is then a mathematical expression defined by the density of events δ times the volume characterized by r_* (see previous demonstrations in Mignan et al. (2007) and Mignan (2011; 2012; 2016a) where simple algebraic expressions were obtained).

In the case of aftershocks, we define the static stress field of the mainshock by

$$\sigma(r) = -\Delta\sigma_0 \left[\left(1 - \frac{c^3}{(r+c)^3}\right)^{-1/2} - 1 \right] \tag{6}$$

with $\Delta\sigma_0 < 0$ the mainshock stress drop, c the crack radius and r the distance from the crack. Eq (6) is a simplified representation of stress change from slip on a planar surface in a homogeneous elastic medium. It takes into account both the square root singularity at crack tip and the $1/r^3$ falloff at higher distances (Dieterich, 1994) (Fig. 1b). It should be noted that this radial static stress field does not represent the geometric complexity of Coulomb stress fields (Fig. 2a). However we are here only interested in the general behavior of aftershocks with Eq. (6) retaining the first-order characteristics of this field (i.e., on-fault seismicity; Fig. 2b), which corresponds to the case where the mainshock relieves most of the regional stresses and aftershocks occur on optimally oriented faults. It is also in agreement with observations, most aftershocks being located on and around the mainshock fault traces in Southern California (Fig. 2c; see section "Observations & Model Fitting"). The occasional cases where aftershocks occur off-fault (e.g., Ross et al., 2017) can be explained by the mainshock not relieving all of the regional stress (King et al., 1994) (Fig. 2d).

For $r_* = r(\sigma = \Delta o_*)$, Eq. (6) yields the aftershock solid envelope of the form:

$$r_*(c) = \left\{ \frac{1}{\left[1-\left(1-\frac{\Delta\sigma_*}{\Delta\sigma_0}\right)^{-2}\right]^{1/3}} - 1 \right\} c = Fc \tag{7}$$

, function of the crack radius *c* and of the ratio between background stress amplitude range Δo_* and stress drop $\Delta\sigma_0$ (Fig. 1c). With $\Delta\sigma_0$ independent of earthquake size (Kanamori and Anderson, 1975; Abercrombie and Leary, 1993) and Δo_* assumed constant, r_* is directly proportional to *c* with proportionality constant, or stress factor, *F* (Eq. 7). Geometrical constraints due to the seismogenic layer width w_0 then yield

$$c(M) = \begin{cases} \left(\frac{S(M)}{\pi}\right)^{1/2} & , S(M) \leq \pi w_0^2 \\ w_0 & , S(M) > \pi w_0^2 \end{cases} \tag{8}$$

with *S* the rupture surface defined by Eq. (4) and *c* becoming an effective crack radius (Kanamori and Anderson, 1975) (Fig. 1d). Note that the factor of 2 (i.e., using w_0 instead of $w_0/2$) comes from the free surface effect (e.g., Kanamori and Anderson, 1975; Shaw and Scholz, 2001).

The aftershock productivity *K*(*M*) is then the activation density δ_+ times the volume $V_*(M)$ of the aftershock solid. For the case in which the mainshock relieves most of the regional stress, stresses are increased all around the rupture (King et al., 1994), which is topologically identical to stresses increasing radially from the rupture plane (Fig. 2a-b). It follows that the aftershock solid can be represented by a volume of contour $r_*(M)$ from the rupture plane geometric primitive, i.e., a disk or a rectangle, for small and large mainshocks respectively. This is illustrated in Figure 3a-b and can be generalized by

$$V_*(M) = 2r_*(M)S(M) + \frac{\pi}{2}r_*^2(M)d \tag{9}$$

where d is the distance travelled around the geometric primitive by the geometric centroid of the semi-circle of radius $r_*(M)$ (i.e., Pappus's Centroid Theorem), or

$$d = \begin{cases} 2\pi\left(c(M) + \frac{4}{3\pi} r_*(M)\right) & , c(M) + r_*(M) \le \frac{w_0}{2} \\ 2w_0 & , c(M) + r_*(M) > \frac{w_0}{2} \end{cases} \quad (10)$$

For the disk, the volume (Eq. 9) corresponds to the sum of a cylinder of radius $c(M)$ and height $2r_*(M)$ (first term) and of half a torus of major radius $c(M)$ and minus radius $r_*(M)$ (second term). For the rectangle, the volume is the sum of a cuboid of length $l(M)$ (i.e., rupture length), width w_0 and height $2r_*(M)$ (first term) and of a cylinder of radius $r_*(M)$ and height w_0 (second term; see red and orange volumes, respectively, in Figure 3a-c). Finally inserting Eqs. (7), (8) and (10) into (9), we obtain

$$K(M) = \delta_+ \begin{cases} \left[\frac{2F}{\sqrt{\pi}} + F^2\sqrt{\pi}\left(1 + \frac{4}{3\pi}F\right)\right] S^{3/2}(M) & , S(M) \le \left(\frac{w_0\sqrt{\pi}}{2(1+F)}\right)^2 \\ \frac{2F}{\sqrt{\pi}} S^{3/2}(M) + F^2 w_0 S(M) & \left(\frac{w_0\sqrt{\pi}}{2(1+F)}\right)^2 < S(M) \le \pi w_0^2 \\ 2F w_0 S(M) + \pi F^2 w_0^3 & , S(M) > \pi w_0^2 \end{cases}$$

(11)

> **Arnaud Mignan 28.11.2017 16:51**
> **Deleted:** (m_0)

which is represented in Figure 3d. Considering the two main regimes only (small versus large mainshocks) and inserting Eq. (4) into (11), we get

$$K(M) = \delta_+ \begin{cases} \left[\frac{2F}{\sqrt{\pi}} + F^2\sqrt{\pi}\left(1 + \frac{4}{3\pi}F\right)\right] \exp\left[\frac{3\ln(10)}{2}(M-4)\right] & , \text{small } M \\ 2F w_0 \exp[\ln(10)(M-4)] + \pi F^2 w_0^3 & , \text{large } M \end{cases} \quad (12)$$

> **Arnaud Mignan 28.11.2017 16:52**
> **Deleted:** (m_0)

which is a closed-form expression of the same form as the original Utsu productivity law (Eq. 1). Note that K and δ_+ are both, implicitly, function of the selected minimum aftershock magnitude threshold m_0.

Here, we predict that the α-value decreases from 3ln(10)/2 ≈ 3.45 to ln(10) ≈ 2.30 when switching regime from small to large mainshocks (or from 1.5 to 1 in base-10 logarithmic scale). It should be noted that Hainzl et al. (2010) observed the same break in scaling in static stress transfer simulations, which corroborates our analytical findings. For large *M*, the scaling is fundamentally the same as in Eq. (4). Since that relation also explains the slope of the Gutenberg-Richter law (see physical explanation given by Kanamori and Anderson (1975)), it follows that $\alpha \equiv \beta$, which is also in agreement with the original formulation of Utsu (1970a; b) (Eq. 3).

2.2. Validation of the Solid Seismicity Postulate

The SSP predicts a step-like spatial behavior of aftershocks for an idealized smooth static stress field (Fig. 4a-b), which is in disagreement with real aftershock observations. A number of studies have shown that the spatial linear density distribution of aftershocks ρ is well represented by a power-law, expressed as

$$\rho(r) \propto r^{-q} \qquad (13)$$

with *r* the distance from the mainshock and *q* the power-law exponent. This parameter ranges over $1.3 \leq q \leq 2.5$ (Felzer and Brodsky, 2006; Lipiello et al., 2009; Marsan and Lengliné, 2010; Richards-Dinger et al., 2010; Shearer, 2012; Gu et al., 2013; Moradpour et al., 2014; van der Elst and Shaw, 2015). Although Felzer and Brodsky (2004) suggested a dynamic stress origin for aftershocks, their results were later on discredited by Richards-Dinger et al. (2010). Most of the studies cited above suggest that the *q*-value is explained from a static stress process (as for the examples of aftershocks shown to be dynamically triggered (e.g., Fan and Shearer, 2016), they are too few to alter the aftershock productivity law and too remote to be consistently defined as aftershocks in cluster methods).

In a more realistic setting, the static stress field must be heterogeneous (due to the occurrence of previous events and other potential stress perturbations). We therefore simulate the static stress field by adding a uniform random component bounded over $\pm\Delta\sigma_*$ following Mignan (2011) (see also King and Bowman, 2003). Note that any deviation above $\Delta\sigma_*$ would be flattened to $\Delta\sigma_*$ over time by temporal diffusion (so-called "historical ghost static stress field" in Mignan, 2016a). Figure 4c shows the resulting stress field and Figure 4d the predicted aftershock spatial density. Adding uniform noise blurs the contour of the aftershock solid, switching the aftershock spatial density from a step function (Fig. 4b) to a power-law (Fig. 4d). We fit Eq. (13) to the simulated data using the Maximum Likelihood Estimation (MLE) method with $r_{min} = r_*$ (Clauset et al., 2009) and find q = 1.96±0.01, in agreement with the aftershock literature.

3. Observations & Model Fitting

3.1. Data

We consider the case of Southern California and extract aftershock sequences from the relocated earthquake catalog of Hauksson et al. (2012) defined over the period 1981-2011, using the nearest-neighbor method (Zaliapin et al., 2008) (used with its standard parameters originally calibrated for Southern California, considering only the first aftershock generation). Only events with magnitudes greater than m_0 = 2.0 are considered (a conservative estimate following results of Tormann et al. (2014); saturation effects immediately after the mainshock are negligible when considering entire aftershock sequences; Helmstetter et al. (2005)).

Arnaud Mignan 28.11.2017 15:39
Deleted: The observed number of aftershocks n produced by a mainshock of magnitude M (for a total of N mainshocks) is shown in Figure 4.

3.2. Aftershock spatial density distribution

Figure 5a represents the spatial linear density distribution of aftershocks $\rho(r)$ for the four largest strike-slip mainshocks in Southern California: 1987 M=6.6 Superstition Hills, 1992 M=7.3 Landers, 1999 M=7.1 Hector Mine, and 2010 M=7.2

El Mayor. The distance between mainshock and aftershocks is calculated as $r = \sqrt{(x - x_0)^2 + (y - y_0)^2}$ with (x, y) the aftershock coordinates and (x_0, y_0) the coordinates of the nearest point to the mainshock fault rupture (as depicted in Figure 2c). The dashed black lines shown in Figure 5a are visual guides to $q = 1.96$, showing that the SSP is compatible with real aftershock observations.

Comparing Figure 5a to Figure 4d suggests that r_* can be roughly estimated from the spatial linear density plot, being the maximum distance r at which the plateau ends, here leading to $r_* \approx 1$ km. This parameter is constant for different large M values since both w_0 and $\Delta\sigma_0$ are constant while $\Delta\sigma_*$ is also *a priori* a constant. We can then estimate the ratio $\Delta\sigma_*/\Delta\sigma_0$ from Eq. (7). However the result is ambiguous due to uncertainties on the width w_0. For $w_0 = \{5, 10, 15\}$ km, we get $\Delta\sigma_*/\Delta\sigma_0 = \{-0.54, -1.01, -1.38\}$.

As for the plateau value $\rho(r < r_*)$, it provides an estimate of the aftershock activation density δ_+ with

$$\delta_+ = \frac{\rho(M, r < r_*)}{\exp[\ln(10)(M - 4)]} \qquad (14)$$

a volumetric density, i.e. the linear density ρ normalized by the mainshock rupture area (Eq. 4). Due to the fluctuations in $\rho(r < r_*)$, δ_+ will be estimated from the productivity law instead (see section 3.3) and $\rho(r < r_*)$ then estimated from Eq. (14) (horizontal dashed colored lines), as detailed below.

It should be noted that we consider only the first-generation aftershocks to avoid ρ heterogeneities from secondary aftershock clusters occurring off-fault. An example of such heterogeneity/anisotropy is illustrated by the Landers-Big Bear case (Fig. 2c; dotted colored curve on Fig. 5a). Those cases are not systematic and therefore not considered in the aftershock productivity law. However they are also due to static stress changes (e.g., King et al., 1994) with the anisotropic effects explainable by Solid Seismicity through the concept of "historical ghost static stress field" (Mignan, 2016a).

3.3. Aftershock productivity law

The observed number n of aftershocks of magnitude $m \geq m_0$ produced by a mainshock of magnitude M (for a total of N mainshocks) in Southern California is shown in Figures 5b (for large $M \geq 6$) and 6a (for the full range $M \geq m_0$). We fit Eq. (1) to the data using the MLE method with the log-likelihood function

$$LL(\theta; X = \{n_i; i = 1, \ldots, N\}) = \sum_{i=1}^{N} [n_i \ln[K_i(\theta)] - K_i(\theta) - \ln(n_i!)] \qquad (15)$$

for a Poisson process, Inserting Eq. (1) in Eq. (15) yields

$$LL(\theta = \{K_0, \alpha\}; X) = \ln(K_0) \sum_{i=1}^{N} n_i + \alpha \sum_{i=1}^{N} [n_i (M_i - m_0)] - K_0 \sum_{i=1}^{N} \exp[\alpha(M_i - m_0)] - \sum_{i=1}^{N} \ln(n_i!) \qquad (16)$$

(note that the last term can be set to 0 during LL maximization). For Southern California, we obtain $\alpha_{MLE} = 2.32$ (1.01 in $\log_{10}$ scale) and $K_0 = 0.025$ when considering large $M \geq 6$ mainshocks only to avoid the issues of scaling break and data dispersion at lower magnitudes. This result, represented by the black solid line on Figure 5b, is in agreement with previous studies in the same region (e.g., Helmstetter, 2003; Helmstetter et al., 2005; Zaliapin and Ben-Zion, 2013; Seif et al., 2017) and with $\alpha = \ln(10) \approx 2.30$ predicted for large mainshocks in Solid Seismicity (Eq. 12). Moreover we find a bulk $\beta_{MLE} = 2.34$ (1.02 in $\log_{10}$ scale) (Aki, 1965), in agreement with $\alpha \equiv \beta$.

Let us now rewrite the Solid Seismicity aftershock productivity law (Eq. 12) by only considering the large M case and injecting $r_* = F w_0$ (by combining Eqs. 7-8). We get

Arnaud Mignan 28.11.2017 10:39
Deleted: first

Arnaud Mignan 28.11.2017 13:46
Deleted: Maximum Likelihood Estimation (

Arnaud Mignan 28.11.2017 13:46
Deleted:)

Arnaud Mignan 28.11.2017 16:16
Deleted: 3

Arnaud Mignan 28.11.2017 15:45
Deleted: , or,

Arnaud Mignan 28.11.2017 13:45
Deleted: with

Arnaud Mignan 28.11.2017 15:46
Deleted: ,

Arnaud Mignan 28.11.2017 16:16
Deleted: 4

Arnaud Mignan 28.11.2017 16:12
Deleted:

Arnaud Mignan 28.11.2017 16:11
Deleted: 04

Arnaud Mignan 28.11.2017 16:12
Deleted: 0.89

Arnaud Mignan 28.11.2017 16:12
Deleted: 3. It should be noted that this approach does not include the case of mainshocks that produce zero aftershock. Therefore we also compute the MLE for the Zero-Inflated Poisson (ZIP) distributior ... [1]

Arnaud Mignan 29.11.2017 10:03
Deleted: =

Arnaud Mignan 28.11.2017 16:14
Deleted: It should be noted that no significant difference is obtained when computing β_{MLE} for background events or aftershocks alone, with $\beta_{MLE} = 2.29$ and 2.35, respectively (0.99 and 1.02 in $\log_{10}$ scale).

$$K(M > M_{break}) = \delta_+\{2r_* \exp[ln(10)(M-4)] + \pi r_*^2 w_0\} \quad (17)$$

The role of w_0 is illustrated in Figure 5b for different values (dashed and dotted curves) and shown to be insignificant for large M values. Therefore Eq. (17) can be approximated to

$$K(M > M_{break}) \approx 2\delta_+ r_* \exp[ln(10)(M-4)] \quad (18)$$

By analogy with Eq. (1), we get

$$\delta_+ = \frac{K_0 \exp[\ln(10)(4-m_0)]}{2r_*} \quad (19)$$

With $r_* \approx 1$ km estimated from $\rho(r)$ (section 3.2) and $K_0 = 0.025$, we obtain $\delta_+ = 1.23$ events/km^3 for $m_0 = 2$. We then get back the plateau $\rho(r < r_*)$ for different M values from Eq. (14), as shown in Figure 5a (horizontal dashed colored lines). Although based on limited data, this result suggests that the activation parameter δ_+ is constant (at least for large M) in Southern California. Note that if $\rho(r < r_*)$ was well constrained, it could have been estimated jointly with r_* from Figure 5a to predict the aftershock productivity law of Figure 5b without further fitting required (hence removing K_0 from the equation, K_0 having no physical meaning in Solid Seismicity).

4. Role of aftershock selection on productivity scaling-break

We tested the following piecewise model to identify any break in scaling at smaller M, as predicted by Eq. (12):

Arnaud Mignan 29.11.2017 11:10
Deleted: also

$$K(M) = \begin{cases} K_0 \dfrac{\exp[\ln(10)(M_{break}-m_0)]}{\exp\left[\frac{3}{2}\ln(10)(M_{break}-m_0)\right]} \exp\left[\frac{3}{2}\ln(10)(M-m_0)\right] & , M \le M_{break} \\ K_0 \exp[\ln(10)(M-m_0)] & , M > M_{break} \end{cases}$$

(20)

Arnaud Mignan 29.11.2017 11:10
Deleted: 16

but with the best MLE result obtained for $M_{break} = m_0$, suggesting no break in scaling in the aftershock productivity data, as observed in Figure 6a. Final parameter estimates are $\alpha_{MLE} = 1.95$ (in $\log_{10}$ scale) and $K_0 = 0.141$ for the full mainshock magnitude range $M \geq m_0$ (dotted line), subject to high scattering at low M values.

We now identify whether the lack of break in scaling in aftershock productivity observed in earthquake catalogues could be an artefact related to the aftershock selection method. We run Epidemic-Type Aftershock Sequence (ETAS) simulations (Ogata, 1988; Ogata and Zhuang, 2006), with the seismicity rate

$$\begin{cases} \lambda(t,x,y) = \mu(t,x,y) + \sum_{i:t_j<t} K(M_i) f(t-t_i) g(x-x_i, y-y_i|M_i) \\ f(t) = c^{p-1}(p-1)(t+c)^{-p} \\ g(x,y|M) = \frac{1}{\pi}\left(de^{\gamma(M-m_0)}\right)^{q-1}\left(x^2+y^2+de^{\gamma(M-m_0)}\right)^{-q}(q-1) \end{cases} \quad (21)$$

Aftershock sequences are defined by power laws, both in time and space (for an alternative temporal function, see Mignan (2015; 2016b); the spatial power-law distribution is in agreement with Solid Seismicity in the case of a heterogeneous static stress field – see section 2.2). μ is the Southern California background seismicity, as defined by the nearest-neighbor method (with same t, x, y and m). We fix the ETAS parameters to θ = {$c = 0.011$ day, $p = 1.08$, $d = 0.0019$ km^2, $q = 1.47$, $\gamma = 2.01$, $\beta = 2.29$, $K_0 = 0.08$}, following the fitting results of Seif et al. (2017) for the Southern California relocated catalog and $m_0 = 2$ (see their Table 1). However, we define the productivity function $K(M)$ from Eq. (20) with $M_{break} = 5$. Examples of ETAS simulations are shown in Figure 6b for comparison with the observed Southern California time series. Figure 6c allows us to verify that the simulated aftershock productivity is kinked at M_{break}, as defined by Eq. (20).

We then select aftershocks from the ETAS simulations with the nearest-neighbor method. Figure 4d represents the estimated aftershock productivity, which has lost the break in scaling originally implemented in the simulations (with an underestimated $\alpha_{MLE} = 2.07$ as observed in the real case for $M \geq m_0$). Note that a

Arnaud Mignan 29.11.2017 11:13
Deleted: ... [2]

Arnaud Mignan 29.11.2017 11:11
Deleted: 16

Arnaud Mignan 5.12.2017 10:12
Deleted: , $K_0 = 0.23$, $\alpha = 2.04$ and $\beta = 2.3$.

Arnaud Mignan 29.11.2017 11:12
Deleted: 16

similar result is obtained when using a windowing method (Gardner and Knopoff, 1974). This demonstrates that the theoretical break in scaling predicted in the aftershock productivity law can be lost in observations due to an aftershock selection bias, all declustering techniques assuming continuity over the entire magnitude range. While such a bias is possible, it yet does not prove that the break in scaling exists. The fact that a similar break in scaling was obtained in independent Coulomb stress simulations (Hainzl et al., 2010) however provides high confidence in our results.

One other possible explanation for lack of scaling break is that our demonstration assumes moment magnitudes while the Southern California catalogue is in local magnitudes. Deichmann (2017) demonstrated that while $M_L \propto M_w$ at large M, $M_L \propto 1.5M_w$ at smaller M values. This could in theory cancel the kink in real data. However the scaling break predicted by Deichmann (2017) occurs at several magnitude units below the geometric scaling break expected by Solid Seismicity, invalidating this second option for mid-range magnitudes M.

5. Conclusions

In the present study, a physical closed-form expression defined from geometric and static stress parameters was proposed (Eq. 12) to explain the empirical Utsu aftershock productivity law (Eq. 1). This demonstration, combined to the previous ones made by the author to explain precursory accelerating seismicity and induced seismicity (Mignan, 2012; 2016b), suggests that most empirical laws observed in seismicity populations can be explained by simple geometric operations on a permanent static stress field. In all these demonstrations, the main physical parameters remain the same, i.e. the activation density δ_+ (also δ_- and δ_0), the background stress amplitude range $\Delta\sigma_*$, and the solid envelope r_* which describes the geometry of the "seismicity solid" (Fig. 3a-b). Further studies will be needed to evaluate whether the δ_+ and $\Delta\sigma_*$ parameters are universal or region-specific and if the same values apply to different types of seismicity at a same location.

Although the Solid Seismicity Postulate (SSP) (Eq. 5) remains to be proven, it is so far a rather convenient and pragmatic assumption to determine the physical parameters that play a first-order role in the behavior of seismicity. The similarity of the SSP-simulated and observed values of the power-law exponent q of the aftershock spatial density distribution suggests that the SSP is a proper approach (Figs. 4d-5a). It is also complementary to the more common simulations of static stress loading (King and Bowman, 2003) and static stress triggering (Hainzl et al., 2010).

Analytic geometry, providing both a visual representation and an analytical expression of the problem at hand (Fig. 3), represents a new approach to try to understand better the behavior of seismicity. Its current limitation in the case of aftershock analysis consists in assuming that the static stress field is radial and described by Eq. (6) (Dieterich, 1994), which is likely only valid for mainshocks relieving most of the regional stresses and with aftershocks occurring on optimally oriented faults (King et al., 1994). More complex, second-order, stress behaviors might explain part of the scattering observed around Eq. (1) (Fig. 6a), such as overpressure due to trapped high-pressure gas for example (Miller et al., 2004 – see also Mignan (2016a) for an overpressure field due to fluid injection). Other $\sigma(r)$ formulations could be tested in the future, the only constraint on generating so-called seismicity solids being the use of the postulated static stress step function of Eq. (5) (i.e., the Solid Seismicity Postulate, SSP).

Finally, the disappearance of the predicted scaling break in the aftershock productivity law once declustering is applied (Fig. 6) indicates that more work is

Arnaud Mignan 5.12.2017 10:19
Deleted: better

Arnaud Mignan 5.12.2017 10:19
Deleted: ing

Arnaud Mignan 4.12.2017 13:39
Deleted: 4

required in that domain. Only a declustering technique that does not dictate a constant scaling at all *M* will be able to identify rather a scaling break really exists or not.

Acknowledgments: I thank N. Wetzler and two anonymous reviewers for their valuable comments.

References

Abercrombie, R. and Leary, P.: Source parameters of small earthquakes recorded at 2.5 km depth, Cajon Pass, Southern California: Implications for earthquake scaling, Geophys. Res. Lett., 20, 1511-1514, 1993.

Aki, K.: Maximum Likelihood Estimate of b in the Formula log N = a-bM and its Confidence Limits, Bull. Earthq. Res. Instit., 43, 237-239, 1965.

Båth, M.: Lateral inhomogeneities of the upper mantle, Tectonophysics, 2, 483-514, 1965.

Clauset, A., Shalizi, C. R. and Newman, M. E. J.: Power-Law Distributions in Empirical Data, SIAM Review, 51, 661-703, doi: 10.1137/070710111, 2009.

Deichmann, N.: Theoretical Basis for the Observed Break in M_L/M_w Scaling between Small and Large Earthquakes, Bull. Seismol. Soc. Am., 107, doi: 10.1785/0120160318, 2017.

Dieterich, J.: A constitutive law for rate of earthquake production and its application to earthquake clustering, J. Geophys. Res., 99, 2601-2618, 1994.

Fan, W. and Shearer, P. M.: Local near instantaneously dynamically triggered aftershocks of large earthquakes, Science, 353, 1133-1136, 2016.

Felzer, K. R. and Brodsky, E. E.: Decay of aftershock density with distance indicates triggering by dynamic stress, Nature, 441, 735-738, doi: 10.1038/nature04799, 2006.

Gardner, J. K. and Knopoff, L.: Is the sequence of earthquakes in Southern California, with aftershocks removed, Poissonian?, Bull. Seismol. Soc. Am., 64, 1363-1367, 1974.

Gu, C., Schumann, A. Y., Baisesi, M. and Davidsen, J.: Triggering cascades and statistical properties of aftershocks, J. Geophys. Res. Solid Earth, 118, 4278-4295, doi: 10.1002/jgrb.50306, 2013.

Gutenberg, B. and Richter, C. F.: Frequency of earthquakes in California, Bull. Seismol. Soc. Am., 34, 185-188, 1944.

Hainzl, S., Brietzke, G. B. and Zöller, G.: Quantitative earthquake forecasts resulting from static stress triggering, J. Geophys. Res., 115, B11311, doi: 10.1029/2010JB007473, 2010.

Hauksson, E., Yang, W. and Shearer, P. M.: Waveform Relocated Earthquake Catalog for Southern California (1981 to June 2011), Bull. Seismol. Soc. Am., 102, 2239-2244, doi: 10.1785/0120120010, 2012.

Helmstetter, A.: Is Earthquake Triggering Driven by Small Earthquakes?, Phys. Rev. Lett., 91, doi: 10.1102/PhysRevLett.91.058501, 2003.

Helmstetter, A., Kagan, Y. Y. and Jackson, D. D. : Importance of small earthquakes for stress transfers and earthquake triggering, J. Geophys. Res., 110, B05S08, doi: 10.1029/2004JB003286, 2005.

Kanamori, H. and Anderson, D. L.: Theoretical basis of some empirical relations in seismology, Bull. Seismol. Soc. Am., 65, 1073-1095, 1975.

King, G. C. P., Stein, R. S. and Lin, J.: Static Stress Changes and the Triggering of Earthquakes, Bull. Seismol. Soc. Am., 84, 935-953, 1994.

King, G. C. P. and Bowman, D. D.: The evolution of regional seismicity between large earthquakes, J. Geophys. Res., 108, 2096, doi: 10.1029/2001JB000783, 2003.

Lin, J. and Stein, R. S.: Stress triggering in thrust and subduction earthquakes, and stress interaction between the southern San Andreas and nearby thrust and strike-slip faults, J. Geophys. Res., 109, B02303, doi: 10.1029/2003JB002607, 2004.

Lippiello, E., de Arcangelis, J. and Godano, C.: Role of Static Stress Diffusion in the Spatiotemporal Organization of Aftershocks, Phys. Rev. Lett., 103, 038501, doi: 10.1103/PhysRevLett.103.038501, 2009.

Marsan, D. and Lengliné, O.: A new estimation of the decay of aftershock density with distance to the mainshock, J. Geophys. Res., 115, B09302, doi: 10.1029/2009JB007119, 2010.

Miller, S. A., Collettini, C., Chiaraluce, L., Cocco, M., Barchi, M. and Kaus, B. J. P.: Aftershocks driven by a high-pressure CO_2 source at depth, Nature, 427, 724-727

Mignan, A., King, G. C. P. and Bowman, D.: A mathematical formulation of accelerating moment release based on the stress accumulation model, J. Geophys. Res., 112, B07308, doi: 10.1029/2006JB004671, 2007.

Mignan, A.: Non-Critical Precursory Accelerating Seismicity Theory (NC PAST) and limits of the power-law fit methodology, Tectonophysics, 452, 42-50, doi: 10.1016/j.tecto.2008.02.010, 2008.

Mignan, A.: Retrospective on the Accelerating Seismic Release (ASR) hypothesis: Controversy and new horizons, Tectonophysics, 505, 1-16, doi: 10.1016/j.tecto.2011.03.010, 2011.

Mignan, A.: Seismicity precursors to large earthquakes unified in a stress accumulation framework, Geophys. Res. Lett., 39, L21308, doi: 10.1029/2012GL053946, 2012.

Mignan, A.: Modeling aftershocks as a stretched exponential relaxation, Geophys. Res. Lett., 42, 9726-9732, doi: 10.1002/2015GL066232, 2015.

Mignan, A.: Static behaviour of induced seismicity, Nonlin. Processes Geophys., 23, 107-113, doi: 10.5194/npg-23-107-2016, 2016a.

Mignan, A.: Reply to "Comment on 'Revisiting the 1894 Omori Aftershock Dataset with the Stretched Exponential Function' by A. Mignan" by S. Hainzl and A. Christophersen, Seismol. Res. Lett., 87, 1134-1137, doi: 10.1785/0220160110, 2016b.

Moradpour, J., Hainzl, S. and Davidsen, J.: Nontrivial decay of aftershock density with distance in Souther California, J. Geophys. Res. Solid Earth, 119, 5518-5535, doi: 10.1002/2014JB010940, 2014.

Ogata, Y.: Statistical Models for Earthquake Occurrences and Residual Analysis for Point Processes, J. Am. Stat. Assoc., 83, 9-27, 1988.

Ogata, Y. and Zhuang, J.: Space-time ETAS models and an improved extension, Tectonophysics, 413, 13-23, doi: 10.1016/j.tecto.2005.10.016, 2006.

Richards-Dinger, K., Stein, R. S. and Toda, S.: Decay of aftershock density with distance does not indicate triggering by dynamic stress, Nature, 467, 583-586, doi: 10.1038/nature09402, 2010.

Ross, Z. E., Hauksson, E. and Ben-Zion, Y.: Abundant off-fault seismicity and orthogonal structures in the San Jacinto fault zone, Sci. Adv., 3, doi: 10.1126/sciadv.1601946, 2017.

Seif, S., Mignan, A., Zechar, J. D., Werner, M. J. and Wiemer, S.: Estimating ETAS: The effects of truncation, missing data, and model assumptions, J. Geophys. Res. Solid Earth, 121, 449-469, doi: 10.1002/2016JB012809, 2017.

Shapiro, S. A. and Dinske, C.: Scaling of seismicity induced by nonlinear fluid-rock interaction, J. Geophys. Res., 114, B09307, doi: 10.1029/2008JB006145, 2009.

Shaw, B. E. and Scholz, C. H.: Slip-length scaling in large earthquakes: Observations and theory and implications for earthquake physics, Geophys. Res. Lett., 28, 2995-2998, 2001.

Shearer, P. M.: Space-time clustering of seismicity in California and the distance dependence of earthquake triggering, J. Geophys. Res., 117, B10306, doi: 10.1029/2012JB009471, 2012.

Toda, S., Stein, R. S., Richards-Dinger, K. and Bozkurt, S.: Forecasting the evolution of seismicity in southern California: Animations built on earthquake stress transfer, J. Geophys. Res., 110, B05S16, doi: 10.1029/2004JB003415, 2005.

Tormann, T., Wiemer, S. and Mignan, A.: Systematic survey of high-resolution b value imaging along Californian faults: inference on asperities, J. Geophys. Res. Solid Earth, 119, 2029-2054, doi: 10.1002/2013JB010867, 2014.

Utsu, T.: Aftershocks and Earthquake Statistics (1): Some Parameters Which Characterize an Aftershock Sequence and Their Interrelations, J. Faculty Sci. Hokkaido Univ. Series 7 Geophysics, 3, 129-195, 1970a.

Utsu, T.: Aftershocks and Earthquake Statistics (2): Further Investigation of Aftershocks and Other Earthquake Sequences Based on a New Classification of Earthquake Sequences, J. Faculty Sci. Hokkaido Univ. Series 7 Geophysics, 3, 197-266, 1970b.

Utsu, T., Ogata,, Y. and Matsu'ura, R. S.: The Centenary of the Omori Formula for a Decay Law of Aftershock Activity, J. Phys. Earth, 43, 1-33, 1995.

van der Elst, N. J. and Shaw, B. E.: Larger aftershocks happen farther away: Nonseparability of magnitude and spatial distributions of aftershocks, Geophys. Res. Lett., 42, 5771-5778, doi: 10.1002/2015GL064734, 2015.

Varnes, D. J.: Predicting Earthquakes by Analyzing Accelerating Precursory Seismic Activity, Pure Appl. Geophys., 130, 661-686, 1989.

Yamanaka, Y. and Shimazaki, K.: Scaling Relationship between the Number of Aftershocks and the Size of the Main Shock, J. Phys. Earth, 38, 305-324, 1990.

Zaliapin, I., Gabrielov, A., Keilis-Borok, V. and Wong, H.: Clustering Analysis of Seismicity and Aftershock Identification, Phys. Rev. Lett., 101, 018501, doi: 10.1103/PhysRevLett.101.018501, 2008.

Zaliapin, I. and Ben-Zion, Y.: Earthquake clusters in southern California I: Identification and stability, J. Geophys. Res. Solid Earth, 118, 2847-2864, doi: 10.1002/jgrb.50179, 2013.

Figures

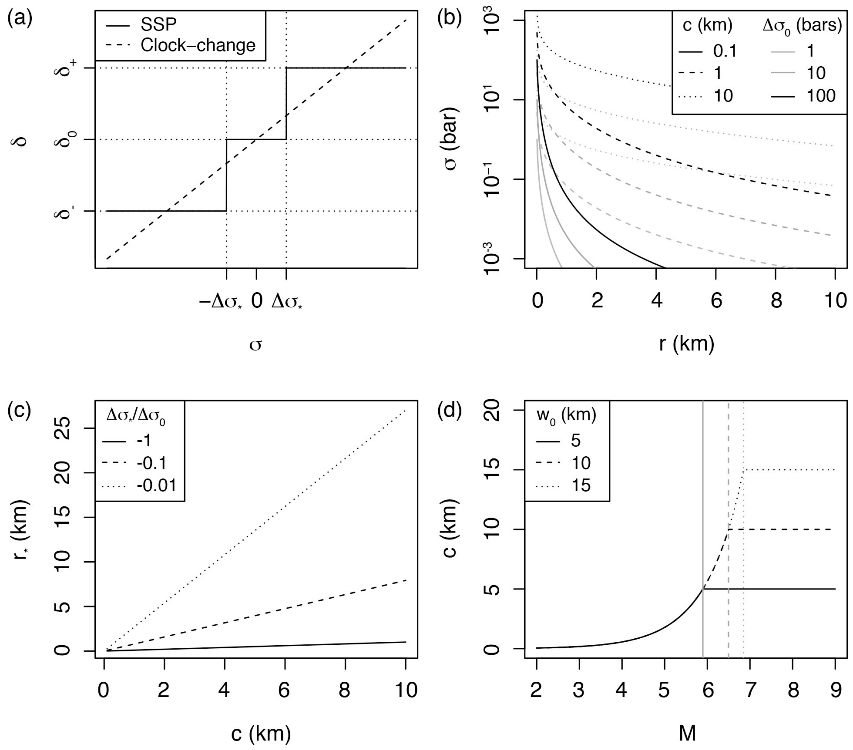

Figure 1. Definition of the aftershock solid envelope in a permanent static stress field: (a) Event density stress step-function δ(σ) (Eq. 5) of the Solid Seismicity Postulate (SSP) in comparison to the linear clock-change model; (b) Static stress σ versus distance *r* for different effective crack radii *c* and rupture stress drops $\Delta\sigma_0$ (Eq. 6); (c) Linear relationship between effective crack radius *c* and aftershock solid envelope radius r_* for different $\Delta\sigma_*/\Delta\sigma_0$ ratios (Eq. 7); (d) Relationship between mainshock magnitude *M* and effective crack radius *c* for different seismogenic widths w_0 (Eq. 8).

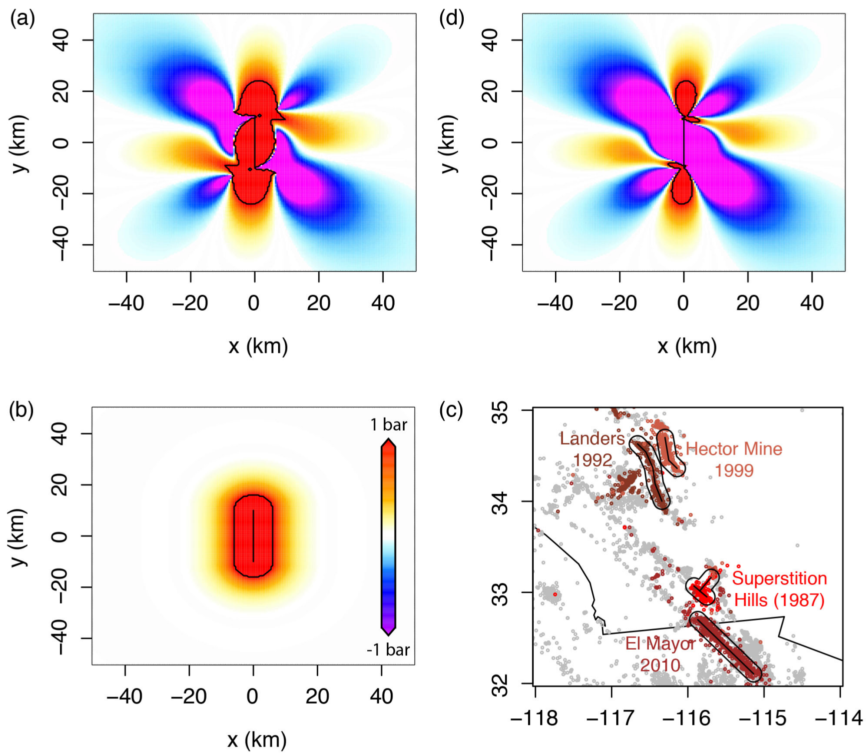

Figure 2. Possible static stress fields and inferred aftershock spatial distribution: (a) Right-lateral Coulomb stress field for optimally oriented faults, where the mainshock relieves all of the regional stresses σ_r = 10 bar, with $\Delta\sigma_0 \approx -Gs/L \approx$ - 10 bar (G = $3.3.10^5$ bar the shear modulus, s = 0.6 m the slip, L = 20 km the fault length, and w = 10 km the fault width); (b) Radial static stress field computed from Eq. (6) with $\Delta\sigma_0$ = -10 bar and $c = \sqrt{(Lw)/\pi}$ for consistency with (a); (c) Aftershock distribution of the largest strike-slip events in the Southern California relocated catalog, identified here as all events occurring within one day of the mainshock (see Data section 3.1); (d) Right-lateral Coulomb stress field for optimally oriented faults, where the mainshock relieves only a fraction of the regional stresses σ_r = 100 bar with $\Delta\sigma_0$ = -10 bar (same rupture as in (a)) – The black contour represents 1 bar in (a), (b) and (d), and a 10 km

distance from rupture in (c). Coulomb stress fields of (a) and (d) were computed using the Coulomb 3 software (Lin and Stein, 2004; Toda et al., 2005).

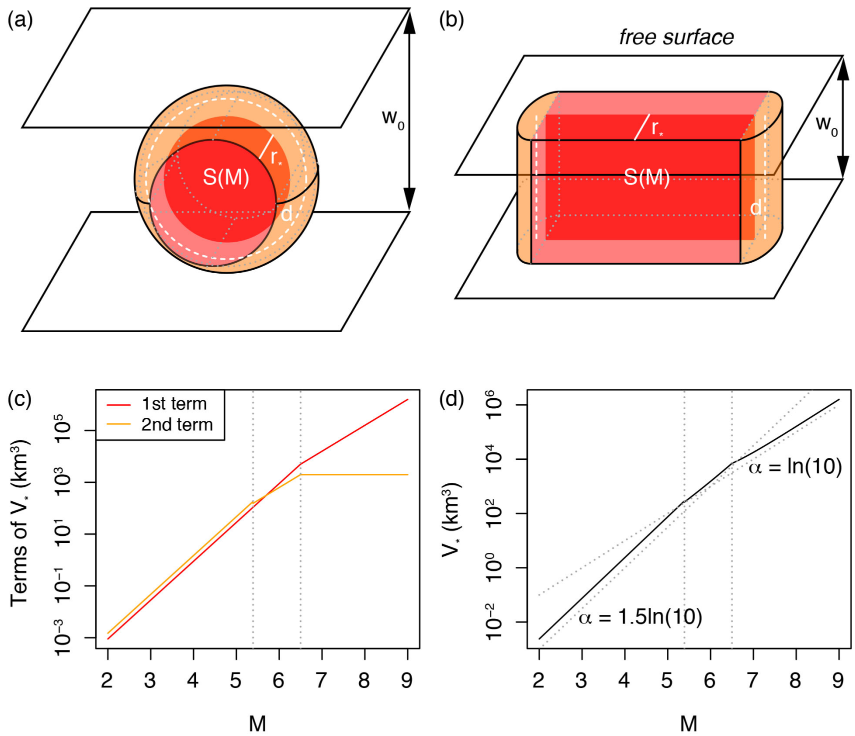

Figure 3. Geometric origin of the aftershock productivity law: (a) Sketch of the aftershock solid for a small mainshock rupture represented by a disk; (b) Sketch of the aftershock solid for a large mainshock rupture represented by a rectangle; (c) Relative role of the two terms of Eq. (9), here with w_0 = 10 km and $\frac{\Delta\sigma_*}{\Delta\sigma_0}$ = -0.1 (to first estimate c and r_* from Eqs. 8 and 7, respectively); (d) Aftershock productivity law (normalized by δ_+) predicted by Solid Seismicity (Eq. 11). This relationship is of the same form as the Utsu productivity law (Eq. 1) for large M (see text for an explanation of the lack

of break in scaling in Eq. 1 for small M). Dotted vertical lines represent M for $c(M) + r_*(M) = \frac{w_0}{2}$ and $S(M) = \pi w_0^2$, respectively.

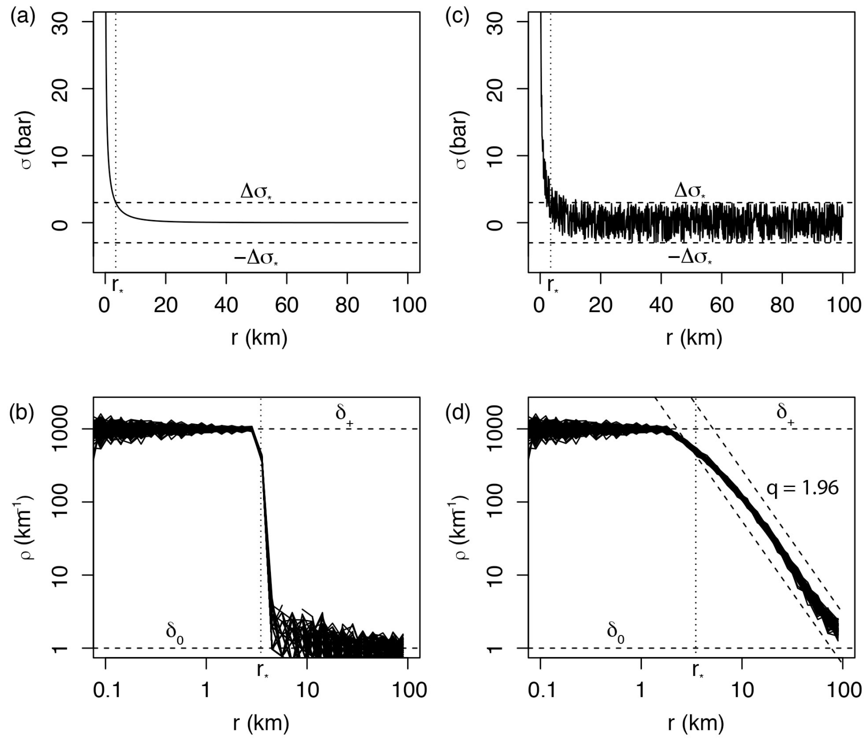

Figure 4. Spatial distribution of aftershocks following the SSP. (a) Smooth static stress field as a function of distance r from the mainshock, with $\Delta\sigma_0$ = -10 bar and c = 10 km (Eq. 6); (b) Step-like aftershock spatial linear density $\rho(r)$ with δ_+ = 1000 events per km, δ_0 = 1 event per km and $\Delta\sigma_*$ = $-0.3\Delta\sigma_0$ (*ad-hoc* ratio yielding r_* = 3.5 km; Eq. (7) – event distances sampled from the $\delta(r)$ distribution, repeated 100 times). Such distribution is not observed in Nature; (c) Same as (a) but with random uniform noise representative of spatial heterogeneities added to the regional stress field; (d) Power-law-like aftershock spatial linear density $\rho(r)$ with power exponent MLE

estimate q = 1.96, representative of real aftershock observations (see Fig. 5a), due to the addition of uniform noise to the static stress field.

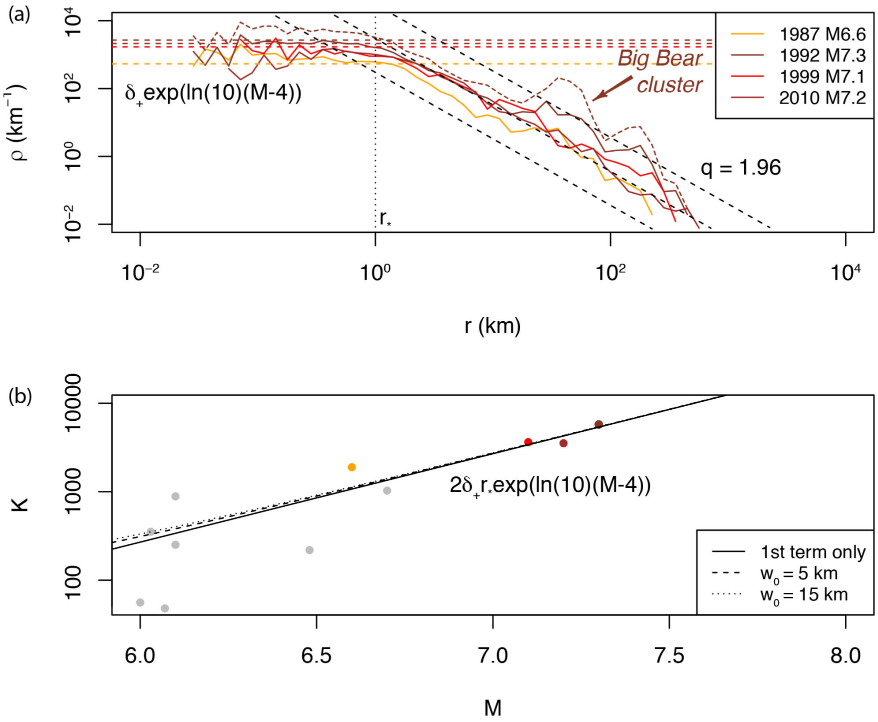

Figure 5. Estimating the Solid Seismicity parameters from the spatial distribution of aftershocks: (a) Spatial linear density distribution $\rho(r)$ of aftershocks for the four largest strike-slip mainshocks in Southern California (with first-generation aftershocks only; the density distribution comprising all aftershocks generated by the Landers mainshock is represented by the dotted curve to illustrate the type of spatial heterogeneity, such as the Big Bear cluster, not considered in the present study – see also Fig. 2c). The Solid Seismicity parameters r_* = 1 km and $\delta_+(m_0 = 2)$ = 1.23 events/km^3 can be retrieved from the observed plateau $\rho(r < r_*)$, in agreement with the SSP (see Fig. 4d). Note that the spatial power-law decay at high r is similar to the one

expected by the SSP in the case of a static stress field with additive uniform noise (expected q = 1.96 represented by the dashed black lines); (b) Aftershock productivity K for M > 6. The curves represent the productivity law as defined by Solid Seismicity (Eq. 17) for different w_0 values (first term only corresponds to w_0 = 0; Eq. 18).

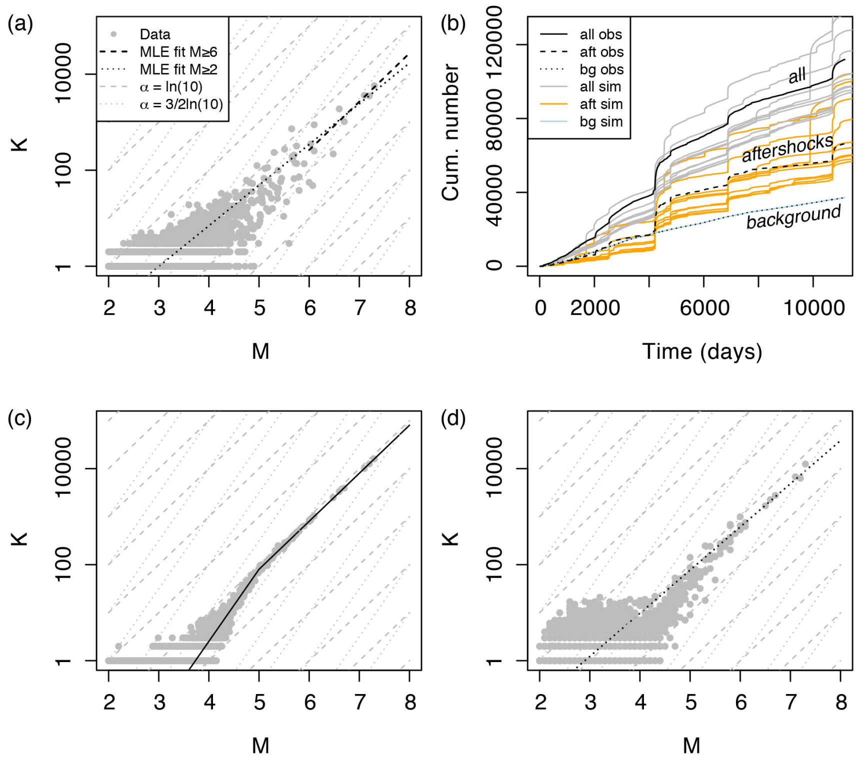

Figure 6. Aftershock productivity defined as the number of aftershocks $K(m_0 = 2)$ per mainshock of magnitude M: (a) Observed aftershock productivity in Southern California with aftershocks selected using the nearest-neighbor method; (b) Seismicity time series with distinction made between background events and aftershocks, observed (“obs”, in black) and ETAS-simulated (“sim”, colored); (c) True simulated aftershock productivity with kink, defined from Eq. (20); (d)

Retrieved simulated aftershock productivity with aftershocks selected using the nearest-neighbor method - Data points in (a), (c) and (d) are represented by grey dots; the model MLE fits are represented by the dashed and dotted black lines for $M \geq 6$ and $M \geq m_0$, respectively; dashed and dotted grey lines are visual guides to $\alpha = 3/2\ln(10)$ and $\ln(10)$, respectively.

Arnaud Mignan 29.11.2017 16:09
Deleted: by Maximum Likelihood Estimation (MLE) method

Arnaud Mignan 4.12.2017 15:05
Deleted: solid

Arnaud Mignan 4.12.2017 15:05
Deleted:

Arnaud Mignan 4.12.2017 15:05
Deleted: the Poisson and Zero-Inflated Poisson distributions

Arnaud Mignan 5.12.2017 10:37
Deleted: a